Nanoscale

High Carrier Mobility in Monolayer CVD-grown MoS2 through Phonon Suppression

Journal:	*Nanoscale*
Manuscript ID	NR-ART-05-2018-004416.R1
Article Type:	Paper
Date Submitted by the Author:	05-Jul-2018

Complete List of Authors:	Huo, Nengjie; Institut de Ciencies Fotoniques, Yang, Yujue; Institut de Ciencies Fotoniques; Guangdong University of Technology Wu, Yu-Ning; University of Florida, Physics Zhang, X.-G.; University of Florida, department of Physics Pantelides, Sokrates; Vanderbilt University, Dept. of Physics and Astronomy Konstantatos, Gerasimos; Institut de Ciencies Fotoniques, ; Institucio Catalana de Recerca i Estudis Avancats,

SCHOLARONE™
Manuscripts

Please do not adjust margins

Nanoscale

ARTICLE

High Carrier Mobility in Monolayer CVD-grown MoS_2 through Phonon Suppression

Received 00th January 20xx,
Accepted 00th January 20xx

DOI: 10.1039/x0xx00000x

www.rsc.org/

Nengjie Huo, †[a] Yujue Yang, †[ab] Yu-Ning Wu, †[cd] Xiao-Guang Zhang, [d] Sokrates T. Pantelides [e] and Gerasimos Konstantatos*[af]

Mobility engineering is one of the most important challenges that determine the optoelectronic performance of two-dimensional (2D) materials. So far, charged-impurity scattering and electrical-contact barriers have been suppressed through high-ƙ dielectrics and seamless contact engineering, giving rise to carrier-mobility improvement in exfoliated 2D semiconducting MoS_2. Here we demonstrate a facile and scalable technique to effectively suppress both Coulomb scattering and electron-phonon scattering via HfO_2 overlayer, resulting in a large mobility improvement in CVD-grown monolayer MoS_2, in excess of 60 $cm^2 V^{-1} s^{-1}$. Surface passivation and suppression of Coulomb scattering can partially contribute to the mobility increase. Interestingly, we correlate the mobility increase with phonon quenching through Raman and temperature-dependent mobility measurements. The experimental method is facile, industrially scalable, and renders phonon engineering an additional leverage towards further improvements in 2D semiconductor mobility and device performance.

Introduction

Benefiting from its direct band gap, strong light-matter interactions, and mechanical flexibility, monolayer MoS_2 has emerged as the most representative and well-studied compound from the class of two-dimensional (2D) transition-metal dichalcogenides (TMDs) class of materials that hold promise to revolutionize electronic and optoelectronic technology.[1-6] One of the most important figures of merit for 2D TMDs is their carrier mobility, which determines to a large extent their performance as transistors or photodetectors. The factors that determine carrier mobility in MoS_2 have, therefore, been extensively investigated: Coulomb scattering by charged impurities, electron-phonon scattering, the role of the electron effective mass as well as the electrical contact are considered the determining factors of mobility in 2D-TMDs devices.[7-11]

For exfoliated monolayer MoS_2, the utilization of high-ƙ dielectric as strongly coupled bottom or top-gate insulator has improved the room temperature mobility, reportedly up to hundreds $cm^2 V^{-1} s^{-1}$ in both single layer and bulk MoS_2 due to the damping of Coulomb scattering from the charged traps or impurities.[12-14] An increase in mobility has also been reported via dielectric engineering using ionic-liquid and polymer gating.[15,16] The Schottky barrier at the metal-semiconductor interface can also limit the TMDs´ extracted mobility and, in view of this, several schemes have been proposed that reduce the contact resistance by avoiding the van der Waals (vdW) gap between the metal and 2D materials, enabling the measurement of the intrinsic mobility of the TMDs.[10,17,18] Along this direction the formation of a seamless contact through the local conversion of MoS_2 underneath the metal contact from the semiconducting 2H phase to the metallic 1T phase,[19,20] has also led to drastic improvements in TMDs-based transistors.[21] Compared to exfoliated MoS_2, CVD-grown monolayer MoS_2 suffers from relatively low carrier mobility due to the numerous defects or grain boundaries as scattering centres.[22-28] So far, significant effort has been expended to improve the mobility through optimized CVD growth recipes, such as annealing on smooth substrates,[27] using metal-organic precursors[28] or oxygen-assisted CVD growth.[29] High-ƙ dielectric screening and use of metallic 1T MoS_2 contacts have also been explored in CVD grown MoS_2.[30-32] Such studies have led to improvements in mobility, with reported values in the range 20-90 $cm^2 V^{-1} s^{-1}$ at room temperature.[27-33]

Compared to the widely reported dielectric engineering that serves to suppress charged-impurity scattering, investigations of suppressing phonon scattering, as another determining factor of mobility in 2D TMDs, has thus far remained elusive. At high and room temperature, the mobility is known to be limited by optical phonon scattering.[8,9] Thus, suppression of phonon scattering on free carriers makes a promising approach for further improvement in room-temperature mobility of CVD

a. *ICFO – Institut de Ciencies Fotoniques, The Barcelona Institute of Science and Technology, Castelldefels, 08860, Barcelona, Spain. E-mail: Gerasimos.konstantatos@icfo.es*
b. *School of Materials and Energy, Guangdong University of Technology, Guangzhou, 510006, China*
c. *National Energy Technology Laboratory, United States Department of Energy, 626 Cochrans Mill Road, P.O. Box 10940, Pittsburgh, Pennsylvania 15236-0940, USA*
d. *Department of Physics and the Quantum Theory Project, University of Florida, Gainesville, FL 32611, USA*
e. *Department of Physics and Astronomy and Department of Electrical Engineering and Computer Science, Vanderbilt University, Nashville, TN 37235, USA*
f. *ICREA – Institució Catalana de Recerca i Estudis Avançats, Lluis Companys 23, 08010 Barcelona, Spain*
† These three authors contributed equally to this work.
Electronic Supplementary Information (ESI) available: [details of any supplementary information available should be included here]. See DOI: 10.1039/x0xx00000x

This journal is © The Royal Society of Chemistry 20xx

Please do not adjust margins

grown 2D TMDs. But till now, effective experimental approaches that can suppress phonon scattering and improve mobility have not been reported in 2D TMDs.

Here, we report on a facile and industrially scalable technique that allows us to significantly quench the phonon mode and thus improve the carrier mobility by more than one order of magnitude in single-layer CVD-grown MoS_2 transistors. This is achieved by depositing atop MoS_2 a thin layer of high-ƙ HfO_2 through atomic layer deposition (ALD) at high temperature (200 ºC). Naturally, the removal of surface adsorbates and suppression of Coulomb scattering due to the dielectric screening can contribute partially to the mobility increase. It is interesting, however, that the homopolar phonon mode is also signigicantly suppressed, evidenced from its softening and weakening as well as the reduced temperature dependence exponent on mobility at room temperataure.

Results

Device scheme and carrier mobility

The CVD monolayer MoS_2 was grown on a SiO_2/Si substrate using a horizontal-tube furnace (see Experimental section for the details of the growth method). The grain size of the single-crystalline MoS_2 areas is over 50 µm as shown in the SEM images (Fig. 1a). The Ti (2 nm)/Au (70 nm) electrodes were fabricated by laser writing lithography and thermal evaporation. The devices were annealed in a glove box at 150 ºC for 1 hour to improve the contact quality. The electrical and optical measurements were performed before and after HfO_2 deposition at room temperature and ambient environmental conditions. Fig. 1b shows a schematic diagram of the monolayer MoS_2 with HfO_2 coverage on top. We fabricated the field effect transistors (FETs) with SiO_2 as the back gate insulator as shown in the inset of Fig. 1c. Large hysteresis is observed in the transfer characteristics of the FETs based on the pristine monolayer MoS_2 when measured in ambient conditions, due to the presence of adsorbates such as H_2O and O_2 acting as charge trapping states (Fig. 1c). Upon HfO_2 deposition, the hysteresis is nearly diminished yielding almost overlapping forward and backward curves due to the removal of surface adsorbates and trap-passivation during annealing process in the ALD chamber, as previously reported for exfoliated MoS_2.[34] Moreover, the ON-current is improved by almost three orders of magnitude and the threshold voltage shifts towards negative back gate owing to electron release by adsorbate desorption.[35] The transconductance (S) defined as $\frac{\partial I_{\rm DS}}{\partial V_{\rm G}}$ is increased after hafnia coverage indicating the improvement of mobility. The carrier mobility can be calculated using the formula: $\mu = \frac{\partial I_{\rm DS}}{\partial V_{\rm G}}(\frac{L}{W C_{\rm i} V_{\rm DS}})$, where L is the channel length, W is the channel width, and C_i is the gate capacitance between the channel and the silicon back gate per unit area, which can be given by equation $C_{\rm i} = \frac{\varepsilon_0 \varepsilon_{\rm r}}{d}$, ε_0 is vacuum dielectric constant, and $\varepsilon_{\rm r}$ (3.9) and d (285 nm) are dielectric constant and thickness of SiO_2, respectively.

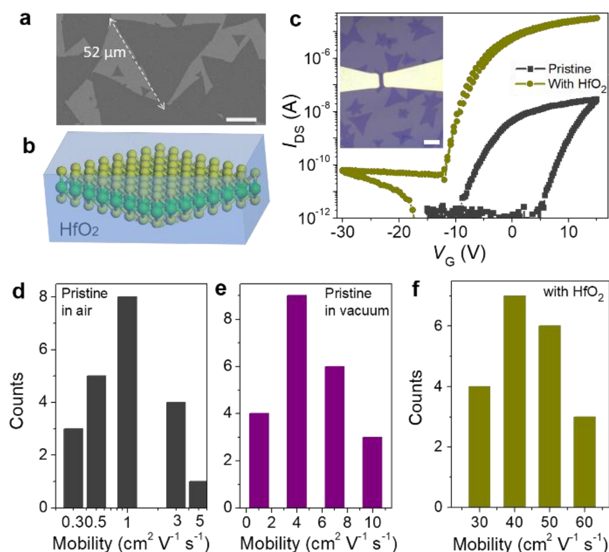

Fig. 1 MoS_2 transistors and carrier mobility. (a) Scanning electron microscopy (SEM) image of CVD-grown monolayer MoS_2. The scale bar is 15 µm. (b) Schematic diagram of HfO_2 deposited MoS_2. (c) Transfer characteristics of pristine and 20 nm HfO_2-covered MoS_2, showing the reduced hysteresis and enhanced ON-state current. The inset is the optical microscopy image of MoS_2 transistors. The scale bar is 10 µm. (d, e) Statistics of mobility in pristine MoS_2 transistors measured in air and in vacuum, respectively. (f) Statistics of mobility in HfO_2-covered MoS_2 transistors.

Several devices based on CVD grown monolayer MoS_2 have been fabricated and measured, and the mobility statistics of pristine MoS_2 is shown in Fig. 1d. The mobility is quite low ranging from 0.3-5 $cm^2 V^{-1} s^{-1}$ similar to previous reports,[24-26,35] due to the surface impurities, defects or traps in MoS_2 and interfaces, as well as the significant phonon scattering at room temperature. The pristine devices were then measured in a sealed high vacuum chamber (10^{-4} mbar), in order to assess the role of the environmental adsorbates, as charge impurity scattering centers, on the mobility of the transistors. Under vacuum, the hysteresis of transfer curves is also suppressed (Supplementary Fig. S1) because of the isolation of air and removal of adsorbates, the mobility is improved to the range of 1-10 $cm^2 V^{-1} s^{-1}$ (shown in Fig. 1e), but it is much smaller than that of the transistors with HfO_2 overlayer (Fig. 1f), this indicates that in addition to the removal of surface adsorbates, other factors such as suppressed coulomb scattering and phonon-electron scattering after HfO_2 coverage can also contribute to the mobility increase. More drastic mobility improvements of nearly one order of magnitude (up to ~60 $cm^2 V^{-1} s^{-1}$) have been observed upon deposition of a thin high-ƙ dielectric HfO_2 (typically 20 nm) via atomic layer deposition (ALD) technique (Fig. 1f). It is noted that the annealing process in the ALD chamber at 200 ºC for around 3 hours is necessary before deposition to fully clean the samples and remove the surface adsorbates. After the HfO_2 deposition, the devices were taken out and cooled down rapidly. It is evident that the presence of hafnia serves not only to remove adsorbates but brings additional benefits in mobility. For example, damping of

This journal is © The Royal Society of Chemistry 20xx

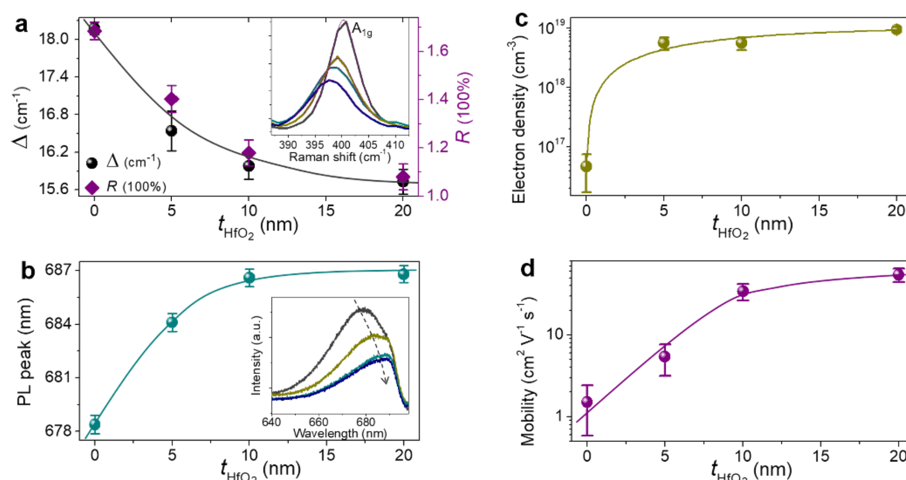

Fig. 2 Correlations between phonon mode and mobility. (a) Raman frequency difference (defined as Δ in cm^{-1}) and Raman intensity ratio (defined as *R* in 100%) between A_{1g} mode and E^1_{2g} mode as a function of HfO_2 thickness. Inset is Raman spectral of A_{1g} mode in MoS_2 as a function of HfO_2 thickness. (b) HfO_2 thickness dependence of PL peak position. Inset is the PL spectrum as function of HfO_2 thickness. (c) HfO_2 thickness dependence of electron density in MoS_2 field effect transistors. (d) HfO_2 thickness dependence of MoS_2 field effect mobility. Error bars in all figures are determined by the average deviations from several different samples.

coulomb scattering due to dielectric screening has been identified and reported as an important determinant factor of mobility in 1D or 2D semiconductors[11]and exfoliated monolayer MoS_2.[7] Here we posit that in addition to this, hafnia also suppresses another determinant mobility factor, that of phonon scattering.

Correlation between phonon mode and mobility

To further investigate the influence of HfO_2 overlayer on the mobility we sought for correlations between phonon mode and mobility in monolayer CVD grown MoS_2. To do so we employed Raman scattering and PL spectral measurements that were correlated with carrier concentration and carrier mobility of MoS_2 as a function of HfO_2 thickness. The pristine MoS_2 has a frequency difference (Δ) of ~18 cm^{-1} between the in-plane E^1_{2g} and the out-of-plane A_{1g} phonon mode, indicative of the monolayer nature of MoS_2.[36] With increasing thickness of HfO_2, the polar optical phonon E^1_{2g} mode remains unaltered (Supplementary Fig. S2), while the homopolar phonon A_{1g} mode softens significantly, as shown in the inset of Fig. 2a, leading to a progressive reduction of Δ to ~16 cm^{-1} (Fig. 2a). With the same trend, the relative intensity of the homopolar phonon (*R:* defined by the intensity ratio of A_{1g} and E^1_{2g} phonon mode) weakens gradually with increasing HfO_2 thickness (Fig. 2a). We also observed a gradual red-shift of the PL peak position by increasing HfO_2 thickness (Fig. 2b), suggestive of a lowered bandgap by around 23 meV upon hafnia coating. The electron doping has been previously reported to soften the homopolar phonon modes.[37] To account for this we plot in Fig. 2c the carrier concentration of the MoS_2 as a function of the HfO_2 thickness, extracted from the transfer curves of MoS_2 transistors of different hafnia thickness (Supplementary Fig. S3). The electron density increases rapidly upon 5nm HfO_2 deposition because of the isolation from air and remains unaltered upon increasing hafnia thickness. Thus the electron density does not follow the gradual shift of both homopolar mode and PL peak and therefore is not the origin of the observations on the PL and Raman spectra. Fig. 2d shows the mobility of MoS_2 as a function of hafnia thickness, the mobility increases gradually up to ~60 $cm^2 V^{-1} s^{-1}$, following closely the phonon mode suppression evolution upon hafnia thickness, indicating a direct correlation between phonon and mobility.

Temperature dependent mobility studies

To further correlate phonon scattering with mobility, we performed temperature dependent electrical transport measurement in CVD grown monolayer MoS_2 transistors. The conductance (*G*), defined as $G = \frac{I_{DS}}{V_{DS}}$ in unit of S, as a function of inverse of temperature (1/*T*) at different back gate values in pristine and HfO_2-covered MoS_2 has been recorded (see Supplementary Fig. S4a and S4b, respectively). In both cases, the conductance variation with temperature can be modelled well in the temperature range of 180-340 K with thermally activated transport: $G = G_0 \exp(-\frac{E_a}{k_B T})$, where G_0 is the fitting parameter, E_a is the activation energy, k_B is the Boltzmann constant. At low temperature below 180 K, the conductance variation weakens due to appearance of the charge hopping transport through localized states.[38] The activation energy in both pristine and HfO_2-covered MoS_2 can be extracted as a function of back gate shown in Fig. 3a. The activation energy is reduced upon HfO_2 deposition, suggestive of more electron doping and less Coulomb scattering in the channel.[39]

Fig. 3b shows the dependence of mobility on temperature of pristine MoS_2. The carrier mobility decreases with decreasing temperature below room temperature (290 K), characteristic of trapped charge impurity scattering.[40] Above room temperature, the mobility also decreases significantly with increasing

This journal is © The Royal Society of Chemistry 20xx

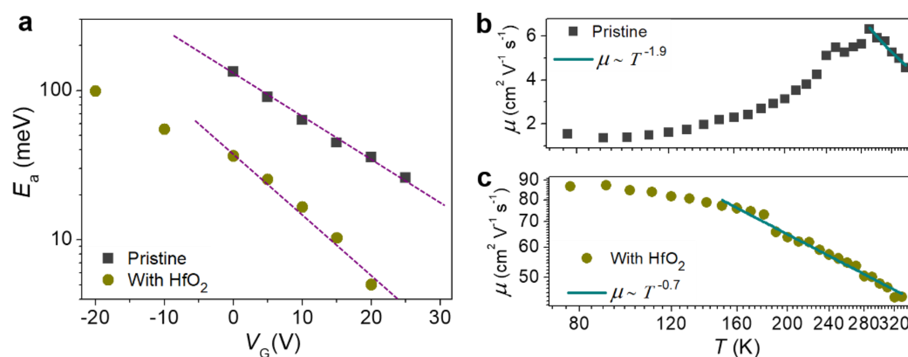

Fig. 3 Temperature dependence of mobility. (a) Activation energy of pristine and HfO_2-covered MoS_2 as a function of back gate voltage. The dash lines are guide to eye (b, c) Temperature dependence of mobility for pristine and HfO_2-covered MoS_2, respectively. The solid lines are the power-law fits.

temperature because of the dominating optical phonon, particularly homopolar phonon, scattering.[9] The temperature dependence of mobility follows the power-law equation: $\mu \sim T^{-\gamma}$, where the exponent γ depends on the electron-phonon coupling strength. The pristine MoS_2 yields an exponent γ of ~1.9, which is in good agreement with theoretical predictions for exfoliated monolayer MoS_2 with γ of 1.69.[9] The large value of γ indicates optical phonon scattering as the dominant limiting factor of the mobility at room temperature conditions. In contrast, we observed a monotonous increase of the mobility as the temperature decreases in the HfO_2-covered MoS_2, shown in Fig. 3c, which can be assigned to the damping of Coulomb scattering from charged defects and traps by the introduction of high-ĸ dielectrics.[11] More importantly, the exponent γ is further reduced to ~0.7 by fitting the mobility dependence on temperature between 150 K and 340 K. The smaller γ value provides direct evidence of the weaker electron-phonon coupling and thus the significant suppression of optical phonon scattering on electrons, which consequently leads to the improvement of the carrier mobility after HfO_2 deposition.

Discussion

From our experiments, we can conclude that not only surface passivation and dielectric screening but also the quenching of homopolar phonons contribute dominantly to the overall mobility increase. One possible origin for the phonon quenching can be due to strain effects. Based on previous studies,[41,42] the covering of oxide layer could introduce 0.3-0.6% tensile train due to the thermal coefficient of expansion (TCE) mismatch between MoS_2 and top oxide layers, resulting in the reduction of bandgap which is consistent with our PL results (Fig. 2b). Recently, the TCE mismatch induced strain engineering has also been demonstrated during CVD growth process of WSe_2[43] and thermal annealing of graphene[44] on various substrates. In our case, it is also possible to introduce tensile strain during the ALD deposition and cooling down process, causing the reduction of bandgap. From the reported theoretical models and the reduction of bandgap, the tensile strain in our MoS_2 is estimated to be ~0.5% with 20 nm HfO_2 on top.[45]

To estimate to which extent tensile strain can affect phonon quenching and thereby mobility in atomically thin 2D MoS_2 we employed density functional theory (DFT) calculations for both MoS_2 mobility and phonon dispersion at different tensile strain values (see Supplementary information for more details). From the calculated phonon dispersions (Supplementary Fig. S5), the tensile stain can lead to the softening of phonons which is consistent with our Raman measurements. The calculated mobility at room temperature as a function of a tensile strain is shown in Table 1. It is evident that tensile strain increases the mobility. To further understand the origin of the increase in the mobility, we extracted the effective mass and the group velocity factor (v_F) by fitting to the band dispersion under different strain conditions, as listed in Table 1. From equation: $\mu = \frac{ev_F}{N\hbar\Delta}\sum_j \tau_{j0}$ (see details in Supplementary Information) and Table 1, we can conclude that the increased mobility caused by tensile strain is attributed partially to the effective mass reduction (in the mobility equation where the factor v_F/Δ is proportional to the inverse effective mass) and most dominantly to the significant damping of the phonon scattering effect, evidenced from the reduction of the complex self-energy $\Sigma_j(\mathbf{k})$ of the effective medium (here $\Sigma_j(\mathbf{k})$ represents the effect of electron-phonon scattering), which is well consistent with the experimental temperature dependence of mobility with reduced exponent γ value. Our results are in good agreement with previous theoretical studies that predict that the electron-phonon coupling can be suppressed by tensile strain leading to large mobility increase in MoS_2.[46] On the other hand, for the experimental value of the strain we estimate have reached, namely 0.5%, the theoretically predicted increase in the carrier

Table 1 The group velocity, Δ, effective mass, average $1/\mathrm{Im}\Sigma$ and mobility (μ) as a function of the strain.

Strain	v_F (10^5 m s^{-1})	Δ ($Å^{-1}$)	m* (m_e)	Average $1/\mathrm{Im}\Sigma$	μ (cm^2 V^{-1} s^{-1})
0%	5.893	0.231	0.466	85.8	106.5
1%	5.711	0.218	0.445	99.1	126.0
2%	5.480	0.188	0.411	112.8	158.4
3%	5.185	0.171	0.395	127.6	185.1

This journal is © The Royal Society of Chemistry 20xx

Please do not adjust margins

mobility is on the order of 15-45%.[45] Thus besides tensile strain, additional factors related to phonon suppression may underscore the high mobility observed herein. For example, the HfO_2 coverage on top or heavy atomic (Hf) adsorption can mechanically quench the homopolar phonons[7] and reduce the exponent γ value. Besides, the remote phonon scattering from both bottom SiO_2 substrate and top HfO_2 dielectric may also play a role in mobility of MoS_2, the optical phonons from SiO_2 substrate can remotely couple with the charge carriers in the MoS_2 channel and reduce the mobility. After HfO_2 deposition, the remote phonon scattering from SiO_2 can be screened to some extent. However, the HfO_2 can meanwhile introduce stronger remote surface scattering because of its higher dielectric constant and lower phonon frequency compared to SiO_2,[47-49] which can decrease mobility again. Thus further theoretical modelling is needed to fully address the suppressed intrinsic phonon scattering and enhanced mobility after HfO_2 overlayer.

Conclusions

In summary, we report CVD grown monolayer MoS_2 transistors with large mobility improvement at room temperature compared to pristine samples by employing a facile method to engineer dielectric environment and phonon suppression via ALD. Upon hafnia covering, the surface impurities scattering and the Coulomb scattering from charged traps or defects are naturally suppressed because of the removal of surface adsorbates and high-ƙ dielectric screening. Most interestingly, the homopolar phonons have been drastically quenched too, leading to the suppression of electron-phonon scattering and further improvement in mobility. These effects contribute to the improvement in mobility, but additional factors such as mechanically phonon quenching by HfO_2 coverage or remote phonon scattering are likely to contribute too. This work demonstrates a facile way to engineer high carrier mobility in CVD grown MoS_2 by suppression of both Coulomb and phonon scattering, and provides a direct correlation between phonon suppression and mobility, paving the way for leveraging additional degrees of freedom in atomically-thin 2D materials in controlling their optoelectronic properties.

Experimental

CVD growth of MoS_2

Monolayer MoS_2 was grown by chemical vapor deposition (CVD) on 285 nm SiO_2/Si substrates. After consecutive cleaning by acetone/2-propanol/DI-water, the substrates were placed face-down above a ceramic boat crucible containing ~5 mg of MoO_3 and loaded into a quartz tube furnace. CVD growth was performed at atmospheric pressure using ultra-high-purity nitrogen as the carrier gas. A second crucible containing ~200 mg of sulfur was located upstream from the growth substrates. The growth recipe is as follows: the system was purged with ultrahigh purity N_2 gas with 500 sccm flow rate for 10 min and heated up to 300 °C for 10 min with 100 sccm, then ramp to the growth temperature of 680 °C with 10 sccm of carrier gas flow, set the temperature of 680 °C for 10 min, then cool it to room temperature naturally. During the cooling down, the carrier gas flow rate was 10 sccm. Below 550 °C, the flow was increased to 300 sccm and opened the furnace for faster cooling down.

Device fabrication and characterization

Metal contacts were fabricated by the laser writing lithography, and Ti (2 nm) and Au (70 nm) electrodes were evaporated by e-beam and thermal evaporation, respectively. Finally, the devices were annealed at 150 °C for 1 hour in glove box to improve the contact quality. After measurement, the devices were deposited by HfO_2 with atomic layer deposition (ALD) technique (Savannah 200, Cambridge Nanotech). The carrier and purge gas was nitrogen (N_2) in which the sample was annealed at 200 °C for around 3 h prior to deposition to remove surface bound adsorbates. After that, the temperature was kept at 200 °C during deposition. Tetrakis (dimethylamino) hafnium and H_2O precursors were used alternatingly with open valve times of 0.15 and 0.015 s, respectively, separated by a 25 s pump time. The process was performed in 200 cycles leading to approximately 20 nm of oxide thickness. All the measurements were performed in ambient conditions using an Agilent B1500A semiconducting device analyzer.

Conflicts of interest

There are no conflicts to declare.

Acknowledgements

We acknowledge financial support from the Spanish Ministry of Economy and Competitiveness, through the “Severo Ochoa” Programme for Centres of Excellence in R&D (SEV-2015-0522), support by Fundacio Cellex Barcelona, and CERCA Programme / Generalitat de Catalunya. Furthermore, the research leading to these results has received funding from the European Union H2020 Programme under grant agreement n°696656 Graphene Flagship. Work at Vanderbilt University and the University of Florida was supported by the U.S. Defense Thread Reduction Agency under Award No. HDTRA1-16-1-0032 (S.T.P.), by the U.S. National Science Foundation under grant ECCS-1508898 (X.G.Z.) and by the McMinn Endowment at Vanderbilt (S.T.P.). Y.Y. acknowledges financial support from the ‘’One-Hundred Talents Program’’ of Guangdong University of Technology (GDUT) and the National Natural Science Foundation of China under Grant No. 11674310.

References

1 B. Radisavljevic, M. B. Whitwick and A. Kis, *ACS Nano*, 2011, **5,** 9934-9938.

Please do not adjust margins

2 L. Britnell, R. M. Ribeiro, A. Eckmann, R. Jalil, B. D. Belle, A. Mishchenko, Y.-J. Kim, R. V. Gorbachev, T. Georgiou, S. V. Morozov, A. N. Grigorenko, A. K. Geim, C. Casiraghi, A. H. Castro Neto and K. S. Novoselov, *Science*, 2013, **340,** 1311-1314.
3 M. M. Furchi, D. K. Polyushkin, A. Pospischil and T. Mueller, *Nano Lett.*, 2014, **14,** 6165-6170.
4 O. Lopez-Sanchez, D. Lembke, M. Kayci, A. Radenovic and A. Kis, *Nat. Nanotechnol*., 2013, **8,** 497-501.
5 X. Cui, G.-H. Lee, Y. D. Kim, G. Arefe, P. Y. Huang, C.-H. Lee, D. A. Chenet, X. Zhang, L. Wang, F. Ye, F. Pizzocchero, B. S. Jessen, K. Watanabe, T. Taniguchi, D. A. Muller, T. Low, P. Kim and J. Hone, *Nat. Nanotechnol*., 2015, **10,** 534-540.
6 K. F. Mak and J. Shan, *Nat. photonics*, 2016, **10,** 216-226.
7 B. Radisavljevic and A. Kis, *Nat. Mater*., 2013, **12,** 815-820.
8 S. Kim, A. Konar, W.-S. Hwang, J. H. Lee, J. Lee, J. Yang, C. Jung, H. Kim, J.-B. Yoo, J.-Y. Choi, Y. W. Jin, S. Y. Lee, D. Jena, W. Choi and K. Kim, *Nat. Commun*., 2012, **3,** 1011.
9 K. Kaasbjerg, K. S. Thygesen and K. W. Jacobsen, *Phys. Rev. B*, 2012, **85,** 115317.
10 L. Wang, I. Meric, P. Y. Huang, Q. Gao, Y. Gao, H. Tran, T. Taniguchi, K. Watanabe, L. M. Campos, D. A. Muller, J. Guo, P. Kim, J. Hone, K. L. Shepard and C. R. Dean, *Science*, 2013, **342,** 614-617.
11 D. Jena and A. Konar, Phys. Rev. Lett., 2007, **98,** 136805.
12 B. Radisavljevic, A. Radenovic, J. Brivio, V. Giacometti and A. Kis, *Nat. Nanotechnol*., 2011, **6,** 147-150.
13 H. Liu and P. D. Ye, *IEEE Electr. Device L*., 2012, **33,** 546-548.
14 Z. Yu, Z.-Y. Ong, Y. Pan, Y. Cui, R. Xin, Y. Shi, B. Wang, Y. Wu, T. Che, Y.-W. Zhang, G. Zhang and X. Wang, *Adv. Mater*., 2016, **28,** 547-552.
15 M. M. Perera, M.-W. Lin, H.-J. Chuang, B. P. Chamlagain, C. Wang, X. Tan, M. M.-C. Cheng, D. Tománek and Z. Zhou, *ACS Nano*, 2013, **7,** 4449-4458.
16 M.-W. Lin, L. Liu, Q. Lan, X. Tan, K. S. Dhindsa, P. Zeng, V. M. Naik, M. M.-C. Cheng and Z. Zhou, *J. Phys. D*, 2012, **45,** 345102.
17 A. Allain, J. Kang, K. Banerjee and A. Kis, *Nat. Mater*., 2015, **14,** 1195-1205.
18 T. Chu and Z. Chen, *ACS Nano*, 2014, **8,** 3584-3589.
19 R. Kappera, D. Voiry, S. E. Yalcin, B. Branch, G. Gupta, A. D. Mohite and M. Chhowalla, *Nat. Mater*., 2014, **13,** 1128-1134.
20 Y.-C. Lin, D. O. Dumcenco, Y.-S. Huang and K. Suenaga, *Nat. Nanotechnol*., 2014, **9,** 391-396.
21 D. Jena, K. Banerjee, and G. H. Xing, *Nat. Mater*., 2014, **13,** 1076-1078.
22 Y.-C. Lin, W. Zhang, J.-K. Huang, K.-K. Liu, Y.-H. Lee, C.-T. Liang, C.-W. Chu and L.-J. Li, *Nanoscale*, 2012, **4,** 6637-6641.
23 C.-C. Huang, F. Al-Saa, Y. Wang, J.-Y. Ou, J. C. Walker, S. Wang, B. Gholipour, R. E. Simpson and D. W. Hewak, *Nanoscale*, 2014, **6,** 12792-12797.
24 Y.-H. Lee, X.-Q. Zhang, W. Zhang, M.-T. Chang, C.-T. Lin, K.-D. Chang, Y.-C. Yu, J. T.-W. Wang, C.-S. Chang, L.-J. Li and T.-W. Lin, *Adv. Mater*., 2012, **24,** 2320-2325.
25 A. M. van der Zande, P. Y. Huang, D. A. Chenet, T. C. Berkelbach, Y. You, G.-H. Lee, T. F. Heinz, D. R. Reichman, D. A. Muller and J. C. Hone, *Nat. Mater*., 2013, **12,** 554-561.
26 G. He, K. Ghosh, U. Singisetti, H. Ramamoorthy, R. Somphonsane, G. Bohra, M. Matsunaga, A. Higuchi, N. Aoki, S. Najmaei, Y. Gong, X. Zhang, R. Vajtai, P. M. Ajayan and J. P. Bird, *Nano Lett*., 2015, **15,** 5052-5058.
27 D. Dumcenco, D. Ovchinnikov, K. Marinov, P. Lazić, M. Gibertini, N. Marzari, O. L. Sanchez, Y.-C. Kung, D. Krasnozhon, M.-W. Chen, S. Bertolazzi, P. Gillet, A. F. Morral, A. Radenovic and A. Kis, *ACS Nano*, 2015, **9,** 4611-4620.
28 K. Kang, S. Xie, L. Huang, Y. Han, P. Y. Huang, K. F. Mak, C.-J. Kim, D. Muller and J. Park, Nature, 2015, **520**, 656-660.
29 W. Chen, J. Zhao, J. Zhang, L. Gu, Z. Yang, X. Li, H. Yu, X. Zhu, R. Yang, D. Shi, X. Lin, J. Guo, X. Bai and G. Zhang, *J. Am. Chem. Soc*., 2015, **137**, 15632-15635.
30 A. Sanne, R. Ghosh, A. Rai, H. C. P. Movva, A. Sharma, R. Rao, L. Mathew and S. K. Banerjee, *Appl. Phys. Lett.*, 2015, **106**, 062101.
31 M. Amani, M. L. Chin, A. G. Birdwell, T. P. O'Regan, S. Najmaei, Z. Liu, P. M. Ajayan, J. Lou and M. Dubey, *Appl. Phys. Lett*., 2013, **102,** 193107.
32 R. Kappera; D. Voiry, S. E. Yalcin, W. Jen, M. Acerce, S. Torrel, B. Branch, S. Lei, W. Chen, S. Najmaei, J. Lou, P. M. Ajayan, G. Gupta, A. D. Mohite and M. Chhowalla, *APL Mater*., 2014, **2,** 092516.
33 H. Schmidt, S. Wang, L. Chu, M. Toh, R. Kumar, W. Zhao, A. H. C. Neto, J. Martin, S. Adam, B. Özyilmaz, and G. Eda, *Nano Lett*., 2014, **14,** 1909-1913.
34 D. Kufer and G. Konstantatos, *Nano Lett*., 2015, **15,** 7307-7313.
35 W. Zhang, J.-K. Huang, C.-H. Chen, Y.-H. Chang, Y. -J. Cheng and L.-J. Li, *Adv. Mater*., 2013, **25,** 3456-3461.
36 H. Li, Q. Zhang, C. C. R. Yap, B. K. Tay, T. H. T. Edwin, A. Olivier and D. Baillargeat, *Adv. Funct. Mater*., 2012, **22,** 1385-1390.
37 B. Chakraborty, A. Bera, D. V. S. Muthu, S. Bhowmick, U. V. Waghmare and A. K. Sood, *Phys. Rev. B*, 2012, **85,** 161403.
38 S. Ghatak, A. N. Pal and A. Ghosh, *ACS Nano*, 2011, **5,** 7707-7712.
39 M.-K. Joo, B. H. Moon, H. Ji, G. H. Han, H. Kim, G. Lee, S. C. Lim, D. Suh and Y. H. Lee, *Nano Lett*., 2016, **16,** 6383-6389.
40 S. M. Sze and K. K. Ng, *Physics of Semiconductor Devices*, (Wiley publishing, 2007).
41 G. Plechinger, F.-X. Schrettenbrunner, J. Eroms, D. Weiss, C. Schüller and T. Korn, *Phys. Status Solidi RRL*, 2012, **6,** 126-128.
42 S. Yu, S. Ran, H. Zhu, K. Eshun, C. Shi, K. Jiang, K. Gu, F. J. Seo and Q. Li, *Appl. Surf. Sci*., 2018, **428,** 593-597.
43 G. H. Ahn, M. Amani, H. Rasool, D.-H. Lien, J. P. Mastandrea, J. W. Ager III, M. Dubey, D. C. Chrzan, A. M. Minor and A. Javey, *Nat. Commun*., 2017, **8,** 608.
44 S.-M. Lee, S.-M. Kim, M. Y. Na, H. J. Chang, K.-S. Kim, H. Yu, H.-J. Lee and J.-H. Kim, *Nano Res*., 2015, **8,** 2082-2091.
45 H. J. Conley, B. Wang, J. I. Ziegler, R. F. Haglund Jr, S. T. Pantelides and K. I. Bolotin, *Nano Lett*., 2013, **13,** 3626-3630.
46 Y. Ge, W. Wan, W. Feng, D. Xiao and Y. Yao, *Phys. Rev. B*, 2014, **90,** 035414.
47 L. Zeng, Z. Xin, S. Chen, G. Du, J. Kang and X. Liu, *Appl. Phys. Lett*. 2013, **103,** 113505.
48 K. Zou, X. Hong, D. Keefer and J. Zhu, *Phys. Rev. Lett.* 2010, **105,** 126601.
49 S. Bhattacharjee, K. L. Ganapathi, H. Chandrasekar, T. Paul, S. Mohan, A. Ghosh, S. Raghavan and N. Bhat, *Adv. Electron. Mater.* 2017, ***3***, 1600358.

This journal is © The Royal Society of Chemistry 20xx

Table of contents

The electron-phonon scattering has been much suppressed in CVD MoS_2, leading to high carrier mobility improvement up to 60 cm^2/Vs.